HHS Public Access

Author manuscript

Biomaterials. Author manuscript; available in PMC 2020 April 01.

Published in final edited form as:

Biomaterials. 2019 April ; 198: 259–269. doi:10.1016/j.biomaterials.2018.08.058.

Electrical stimulation increases hypertrophy and metabolic flux in tissue-engineered human skeletal muscle

Alastair Khodabukus[1], **Lauran Madden**[1], **Neel K. Prabhu**[1], **Timothy R. Koves**[2], **Christopher P. Jackman**[1], **Deborah M. Muoio**[2], and **Nenad Bursac**[1,*]

[1]Department of Biomedical Engineering, Duke University, Durham, NC, USA

[2]Duke Molecular Physiology Institute, Duke University, Durham, NC, USA

Abstract

In vitro models of contractile human skeletal muscle hold promise for use in disease modeling and drug development, but exhibit immature properties compared to native adult muscle. To address this limitation, 3D tissue-engineered human muscles (myobundles) were electrically stimulated using intermittent stimulation regimes at 1Hz and 10Hz rate. Dystrophin in myotubes exhibited mature membrane localization suggesting a relatively advanced starting developmental maturation. One-week stimulation significantly increased myobundle size, sarcomeric protein abundance, calcium transient amplitude (~2-fold), and tetanic force (~3-fold) resulting in the highest specific force generation (19.3mN/mm^2) reported for engineered human muscles to date. Compared to 1Hz electrical stimulation, the 10Hz stimulation protocol resulted in greater myotube hypertrophy and upregulated mTORC1 and ERK1/2 activity. Electrically stimulated myobundles also showed a decrease in fatigue resistance compared to control myobundles without changes in glycolytic or mitochondrial protein levels. Greater glucose consumption and decreased abundance of acetylcarnitine in stimulated myobundles indicated increased glycolytic and fatty acid metabolic flux. Moreover, electrical stimulation of myobundles resulted in a metabolic shift towards longer-chain fatty acid oxidation as evident from increased abundances of medium- and long-chain acylcarnitines. Taken together, our study provides an advanced *in vitro* model of human skeletal muscle with improved structure, function, maturation, and metabolic flux.

Keywords

human skeletal muscle; electrical stimulation; dystrophin; tissue engineering; hypertrophy; organ-on-a-chip

*Corresponding author: Prof. Nenad Bursac, 101 Science Drive, FCIEMAS 1427, Durham, NC27708-90281, phone: 1-919-660-5510, fax: 1-919-684-4488, nbursac@duke.edu.

Data availability

All data supporting the results of these studies are available within the paper, supplemental materials or upon request.

Introduction

Healthy skeletal muscle function is essential for respiration, locomotion and metabolic homeostasis but can be compromised due to aging and genetic, neuromuscular, and metabolic diseases [1–5]. Despite decades of progress, our ability to treat devastating muscle diseases has been relatively limited, in part due to the failure of small animal models to accurately replicate human disease and predict clinically relevant drug responses [6, 7]. The ability to engineer high-fidelity *in vitro* models of human skeletal muscle would significantly advance studies of muscle biology and diseases and allow high-throughput drug development applications in a patient-specific manner. The physiological relevance and predictive power of such assays would be critically dependent on the ability to engineer muscle tissues with mature structural and functional properties [8–15].

We have previously shown that contractile function and maturity of rodent engineered skeletal muscle tissues can be improved via mesoscopic hydrogel molding [16], optimization of starting extracellular matrix protein composition [17], biochemical signaling [18], and dynamic culture Recently, we further refined these methodologies to engineer the first functional human skeletal muscle tissues made from primary myoblasts [19] or pluripotent stem cells [20], termed myobundles. Myobundles recapitulate many of the functional and morphological properties of native muscle and show clinically relevant responses to various drugs that promote or decrease muscle function [19]. However, the resulting myofiber size and isometric contractile properties of myobundles are still inferior to those of native adult muscle indicative of incomplete muscle maturation [19, 21].

Complete skeletal muscle development and maintenance of adult muscle function and mass requires functional innervation. Absence of electrical activity *in utero,* via denervation or paralysis, prevents full maturation and growth of skeletal muscle [22–25]. In adult muscle, denervation results in progressive muscle atrophy which ultimately yields myofibers of similar sizes to those reported in engineered tissues [26–28]. In addition to regulating muscle mass and size, the frequency and number of electrical stimuli regulates the contractile and metabolic phenotype of skeletal muscles [29–34]. Electrical stimulation of 2D human myotubes has been shown to increase myogenic differentiation and alter metabolic substrate utilization [35, 36]. However, performing long-term electrical stimulation studies in 2D cell culture is hindered by the rapid myotube detachment from the underlying substrate [37]. In rodent myogenic cell lines and primary cells, electrical stimulation has been shown to increase engineered muscle force, protein expression, and differentiation markers [37–42]. However, the effects of electrical stimulation on tissue structure and contractile and metabolic function are yet to be studied in functional human tissue-engineered muscles.

Here, we sought to improve the structural and functional properties of our human engineered muscle tissues via use of chronic intermittent electrical stimulation at two frequencies (1Hz and 10Hz). We found that electrical stimulation increases myobundle maturation and force production independent of frequency, but that higher stimulation frequency induces greater myofiber hypertrophy, shortens contractile relaxation time, and promotes shift to a more mature metabolic substrate utilization. With improved structural and functional properties,

electrically stimulated human myobundles represent a promising *in vitro* platform for human disease modeling and drug development applications.

Methods

Human myoblast isolation

Nine human skeletal muscle samples (aged 8 to 34, 5 male and 4 female donors) were obtained through standard needle biopsy or surgical waste from donors under informed consent on Duke University IRB protocols (Pro00048509 and Pro00012628). Muscle samples were minced and digested with 0.05% trypsin for 30 min at 37 °C. Isolated cells were centrifuged and resuspended in growth media (GM, consisting of low-glucose DMEM, 10% fetal bovine serum, supplemented with SkGM bulletkit minus gentamycin and insulin (Lonza) and then preplated for 2 hrs to decrease fibroblast numbers. After pre-plating, cells were seeded onto to Matrigel (BD Biosciences) coated flasks and expanded by passaging upon reaching 70% confluence. At passage 4, cells were detached and used to fabricate myobundles.

Engineered myobundle formation

Three-dimensional engineered muscle tissues (myobundles) were formed within polydimethylsiloxane (PDMS) molds containing two semi-cylindrical wells (7 mm long, 2 mm diameter), cast from 3D-machined Teflon masters, as described previously [19, 20, 43]. PDMS molds were coated with 0.2% (w/v) pluronic F-127 (Invitrogen) for 1 h at room temperature to prevent hydrogel adhesion. Laser-cut Cerex® frames (9×9 mm^2, 1 mm wide rim) positioned around the 2 wells served to anchor bundle ends and facilitate handling and implantation. Specifically, a cell solution (7.5×10^5 cells in 17.2 μl media per bundle + 0.5μl 80ug/ml aprotinin in water + 2 μl of 50 U/ml thrombin in 0. 1% BSA in PBS) and a gelling solution (11 μl media + 10 μl Matrigel + 10 μl of 20 mg/ml Fibrinog en in DMEM) were prepared in separate vials on ice for up to six myobundles per vial. Aprotinin was included in the cell solution to reduce excessive fibrinolysis [44]. Gelling solution was added to the cell solution and mixed thoroughly, then each bundle was individual pipetted within the PDMS mold and onto the frame. Cell/hydrogel mixture was injected into the PDMS wells and polymerized at 37 °C for 30 min. Formed iSKM bundles were dynamically cultured on a rocker and fed with GM supplemented with 1.5 mg/mL 6-aminocaproic acid (ACA, Sigma) to reduce fibrinolysis for 4 days. Media was then switched to differentiation media consisting of low-glucose DMEM, supplemented with 2% horse serum, 100μM L-carnitine, 5μM palmitic acid, 5μM sodium oleate and 2mg/mL ACA with media changed daily.

Electrical stimulation of myobundles

Electrical stimulation was performed between week 1 and 2 of myobundle differentiation (Fig S1A) using 1-hour stimulation bouts separated by 7-hour rests. Specifically, myobundles were continuously electrically stimulated at 1Hz (Fig S1B) or with a 0.5 second, 10Hz pulse train every 5 seconds (Fig S1C), thus delivering the same total number of stimulation pulses. The 1Hz and 10Hz stimulation frequencies were chosen based on a large number of 2D studies in human [35, 36] and C2C12 [45, 46] myotubes utilizing a

similar 1Hz protocol and 3D studies in primary rat [41] and C2C12 [37–40, 47] myotubes using similar 10Hz protocols. The total numbers of impulses delivered by the two protocols were kept constant to ensure that observed effects can be primarily attributed to changes in stimulation frequency [33]. During electrical stimulation, myobundles were placed between parallel carbon electrodes in a custom-made PDMS chamber (Fig S1E). Electrical stimulation protocols were programmed using a custom-made pulse-generating Labview program. Electrical impulses delivered to myobundles were bipolar with 70mA amplitude and 2 ms duration and were delivered using a D330 Multistim system (Digimeter Limited).

Imaging of calcium transients

Myobundles expressing the MHCK7-gCaMP6 reporter were non-destructively monitored for calcium transients prior to isometric contractile testing as described previously [9, 19]. A live imaging chamber with heated enclosure was used to maintain cells in physiological conditions during recording. Myobundles were placed in sterile Tyrode's solution in a custom-designed glass-bottom bath containing carbon electrodes for stimulation. Fluorescent images were acquired through a FITC filter set at 50 fps rate under 4X magnification using an Andor iXon camera affixed to a Nikon microscope. Video analysis was performed using Andor Solis software and relative changes in fluorescence signal were calculated by F/F = (Peak-Trough)/(Trough-Background).

Measurement of isometric contractile properties

Electrically or chemically stimulated contractile force generation in myobundles was measured using a custom force measurement set-up as previously described [8, 9, 17, 19, 20]. Briefly, single myobundles were transferred to the bath of the force measurement set-up, maintained at 37°C. One end of the bundle was secured by a pin to an immobile PDMS block and the other end was attached to a PDMS float connected to the force transducer mounted on a computer-controlled motorized linear actuator (Thor Labs). The sides of the frame were cut to allow myobundle stretch by the actuator and isometric measurement of contractile force. Initially, the myobundle was set to its baseline length using the motorized linear actuator. To assess the force-length relationship, myobundle was stretched by 2% of its culture length then stimulated by a 40 V/cm, 10 ms electrical pulse using a pair of platinum electrodes and the twitch force was recorded. At 12% stretch, 1 s long stimulations at 1, 5, 10, and 20 Hz were applied and the subsequent contractile force was recorded to assess the force-frequency relationship. Contractile force traces were analyzed for peak twitch or tetanus force, time to peak twitch, and half relaxation time using a custom MATLAB program

Immunohistochemistry

Cell monolayers were fixed in 4% paraformaldehyde in PBS for 10 min and myobundles were fixed in 2% paraformaldehyde in PBS overnight at 4° C. Following fixation, samples were washed in PBS then blocked in 5% chick serum with 0.2% Triton-X 100. Primary antibodies were applied at optimized concentrations for 45mins prior to application of fluorescently labeled secondary antibodies for 45 mins. Images were acquired using a Leica SP5 inverted confocal microscope and analyzed using ImageJ. Primary and secondary antibody information can be found in supplementary Table 1.

Western Blotting

Western blotting was performed as described previously [19, 43, 48]. Briefly, protein was isolated in RIPA lysis and extraction buffer with protease inhibitor (Sigma) phosphatase inhibitor cocktail (Roche) and protein concentration determined by BCA assay (Thermofisher). Western blot was performed using Bio-Rad Mini-PROTEAN gels and transferred using a Pierce 2000 powerblot semi-dry transfer system (Thermofisher). Primary antibodies were applied overnight 4^0 C before application of HRP-conjugated anti-mouse (1:20,000) and HRP conjugated anti-rabbit was purchased from SCBT (1:5000). Chemiluminescence was performed using Clarity Western ECL substrate (Bio-Rad). Images were acquired using a Bio-Rad Chemidoc and analyzed using ImageJ.

Quantitative RT-qPCR

RNA was isolated from myobundles using the Aurum Total RNA Mini Kit (Bio-Rad) and then reverse-transcribed using the iScript cDNA Synthesis Kit (Bio-Rad). Quantitative RT-PCR for muscle related genes was performed with iTaq Universal SYBR Green Supermix (Bio-Rad) according to manufacturer's instructions. Primer information can be found in Supplementary Table 2.

Metabolomics—Two-week myobundles were snap frozen in liquid nitrogen immediately following the last bout of electrical stimulation. Acylcarnitines and amino acids were analyzed by flow injection tandem mass spectrometry using sample preparation methods described previously [49, 50]. The data were acquired using a Waters AcquityTM UPLC system equipped with a TQ (triple quadrupole) detector and a data system controlled by MassLynx 4.1 operating system (Waters, Milford, MA). (MS/MS).

Statistics—Data are expressed as mean ± SEM. Statistically significant differences were determined by one-way ANOVA with Tukey's *post hoc* test and $p < 0.05$ was considered significantly different.

3. Results

3.1 Electrical stimulation promotes growth and structural maturation of myobundles

To investigate the effects of simulated exercise on engineered human muscle structure and function, we applied 1-week electrical field stimulation to myobundles that had been differentiated for 7 days (Sup. Fig 1A). Electrical stimulation was applied in 1-hour bouts separated by 7-hour pauses using a continuous 1Hz train or a 0.5 second 10Hz train applied every 5 seconds to ensure that the same number of electrical impulses were delivered by both protocols (Sup. Fig 1B and C). Following 7-day stimulation, myobundles were collected and analyzed by immunohistology and contractile force testing.

From immunostaining analyses, we found that the number of nuclei in transverse cross-sections increased 1.5-fold compared to non-stimulated controls (CTL: 464 ± 24, 1Hz: 689 ± 52, 10Hz 699 ± 42, Fig 1A and C). Electrical stimulation also increased the size of the entire muscle bundle as evident from a 1.8-fold increase in myobundle cross-sectional area (CTL: 0.10 ± 0.004mm^2, 1Hz: 0.17 ± 0.013mm^2, 10Hz: 0.18 ± 0.012mm^2, Fig 1B and D)

and resulted in a 1.6-fold increase in the total F-actin area (primarily labeling muscle cells [8, 19, 20]) compared to non-stimulated controls (CTL: 0.08 ± 0.003mm^2, 1Hz: 0.14 ± 0.010mm^2, 10Hz: 0.15 ± 0.011mm^2).

In contrast to developmentally immature cytoplasmic localization of dystrophin in 2D cultures (Fig S2A), also reported in previous studies [51, 52], all cross-sectional (Fig 2A) and longitudinal (Fig S2B) staining of 3D myobundles demonstrated mature localization of dystrophin in myotube membranes, which allowed precise quantification of myotube cross-sectional area and diameter. We found that myotube cross-sectional area (CTL: 49.0 ± 0.97μm^2; 1Hz: 92.7 ± 3.05μm^2; 10Hz: 110.2 ± 3.32μm^2, Fig 2B) and diameter (CTL: 9.9 ± 0.10μm; 1Hz: 13.1 ± 0.20μm; 10Hz: 14.4 ± 0.2μm, Fig 2C) significantly increased with electrical stimulation, which was further evident from a rightward shift in myotube diameter distribution (Fig 2D). The 10Hz stimulation showed the largest increase ($P<0.001$) resulting from reduced proportion of myotubes with small diameters (4–8μm) and increased proportion of the largest myotubes (>20μm, Fig 2D).

Electrical stimulation also promoted myobundle sarcomeric organization and maturity as evidenced from increased proportion of myotubes with sarcomeric α-actinin$^+$ cross-striations (Fig 3A and B) and 20% increased myotube length (CTL: 468 ± 14.7μm; 1Hz: 577 ± 20.6μm; 10Hz: 549 ± 21.8μm, Fig 3C). Consistent with immunostaining results, western blot analysis showed that electrical stimulation upregulated expression of several sarcomeric proteins including dystrophin, myosin heavy chain, and sarcomeric α-actinin (Fig. 3D and E).

Protein synthesis in skeletal muscle is regulated by the protein kinase mTOR which interacts with several proteins to form two complexes: mTOR complex 1 (mTORC1) containing raptor and mTOR complex 2 (mTORC2) containing rictor [53, 54]. Specifically, mTORC1 activity is required for and correlates with the degree of muscle hypertrophy in response to exercise in rodents and humans [55–58]. Therefore, we analyzed the phosphorylation of mTOR-related kinases immediately following the last bout of electrical stimulation in 2-week myobundles (Fig 4A and B). We found that electrical stimulation significantly increased mTORC1 activity, measured by S6K phosphorylation, in a frequency-dependent manner. Frequency dependent upregulation was also found for mTOR phosphorylation at serine 2448, a marker of both mTORC1 and mTORC2 activation, as well as phosphorylation of ERK1/2, a protein kinase that can regulate mTORC1 activity [59]. Phosphorylation of Akt at serine 473, a positive regulator of mTORC1 activity and a marker of mTORC2 activity [53, 60, 61], was increased similarly by both electrical stimulation regimens, while the phosphorylation of AMPK, a negative regulator of mTORC1 that is activated during energy stress [62], was unchanged by stimulation. Overall, this protein kinase signaling analysis revealed upregulated activation of the anabolic mTOR, S6K, Akt and ERK1/2 pathways.

3.2 Electrical stimulation increases force generation in myobundles

To assess if the stimulation-induced changes in myobundle and myotube structure had effect on muscle function, we measured twitch and tetanic forces of contraction (Fig 5A). For each of the nine donors tested, electrical stimulation improved myobundle contractile force (Fig

5B) yielding a 3-fold higher average twitch (CTL: 0.5 ± 0.03mN; 1Hz: 1.7 ± 0.13mN; 10Hz: 1.5 ± 0.16mN, Fig 5C) and tetanic (CTL: 0.9 ± 0.07mN, 1Hz: 3.4 ± 0.18mN, 10Hz: 3.2 ± 0.19mN, Fig 5D) forces compared to unstimulated control. Specific force (peak tetanic force divided by myobundle cross-sectional area), a marker of muscle maturity, was increased in similarly fashion (CTL: 9.1 ± 0.38mN/mm^2; 1Hz: 19.3 ± 0.63mN/mm^2; 10Hz: 18.9 ± 0.69mm^2, Fig 5E). The higher specific force indicated that the increased absolute force production was a result of not only increased myobundle and F-actin cross-sectional areas, but also possible changes in calcium handling.

3.3 Electrical stimulation increases calcium transient amplitude and alters contractile kinetics of myobundles

To determine if the increase in muscle force generation was related to increases in calcium transient amplitude, we transduced myoblasts with the genetic indicator of intracellular Ca^{2+} concentration, gCaMP6, driven by a muscle-specific promoter, MHCK7, as previously described [9, 19, 20]. From normalized changes in gCaMP6 fluorescence intensity (F/F), we found that electrical stimulation of myobundles resulted in a 2-fold increase in Ca^{2+} transient amplitude (Fig 6A and B). We next determined if this increase was accompanied by changes in twitch kinetics (Fig 6C), a classical marker of muscle fiber type and developmental maturity. While electrical stimulation had no effect on time-to-peak tension (TPT, Fig 6D), half-relaxation time (1/2RT, CTL: 236 ± 13.3msec, 1Hz: 244 ± 6.0msec, 10Hz: 192 ± 10.5msec, Fig. 6E) was significantly shortened by 10Hz stimulation. Additionally, 90% decay time (CTL: 534 ± 29.6msec, 1Hz: 414 ± 14.0msec, 10Hz: 351 ± 7.8msec, Fig 6F) was signif icantly shortened in frequency-dependent manner. Relaxation rates of cytoplasmic calcium transient are regulated, in part, by Ca^{2+} sequestration by calsequestrin, re-uptake to the sarcoplasmic reticulum by SERCA pump, and outflow through sarcolemma via PMCA. To determine if electrical stimulation induced changes in the expression of related Ca^{2+} handling genes, we performed qRT-PCR. In agreement with the faster relaxation kinetics, expressions of PMCA and the fast calsequestrin (CSQ1) and SERCA (SERCA1) isoforms were increased in the 10Hz stimulation group (Fig 6G).

3.4 Electrical stimulation decreases fatigue resistance in myobundles

We next determined if electrical stimulation induced changes in fatigue resistance, along with changes in force generation and calcium handling. Fatigue was measured as the loss of force generation during a continuous 30-second tetanic contraction (Fig 7A). Electrical stimulation increased fatigability of myobundles as evidenced by a larger loss of force at the end of a 30-s contraction (CTL: −55.8 ± 3.03%, 1Hz: −77.7 ± 1.59, 10Hz: −81.3 ± 2.31%, Fig 7B). Typically, decreased fatigue resistance is associated with increased glycolytic metabolism or decreased oxidative metabolism. To determine if electrical stimulation increased glucose consumption, we measured media concentrations of glucose and lactate, a byproduct of anaerobic glycolysis, following 24-hour culture with and without stimulation. Glucose metabolism of electrically stimulated myobundles was increased as shown by decreased media concentration of glucose (Fig 7C) and increased concentration of lactate (Fig 7D). To determine if this increase in glucose consumption was associated with increased expression of glucose transporter proteins, we measured levels of the 2 major glucose transporters in skeletal muscle, GLUT1 and GLUT4. Furthermore, to determine if

changes in fatigability resulted from changes in mitochondrial content, we assessed the expression of mitochondrial enzymes Complex III and V (Fig 7E). We found no significant effects of electrical stimulation on the expression of GLUT1 and GLUT4 proteins or mitochondrial enzymes Complex III and V (Fig 7F).

3.5 Electrical stimulation alters intracellular acylcarnitine species profile and amino acid levels

We next performed intracellular metabolomic analyses to determine if electrical stimulation of myobundles caused changes in their metabolic flux and substrate utilization. Carnitine regulates mitochondrial fatty acid import and oxidation and thus metabolic substrate utilization can be assessed by changes in carbon length and abundance of acylcarnitine species [50]. We thus profiled acylcarnitine species immediately following the last bout of electrical stimulation (Fig 8 and Supplementary table 3) and found that, consistent with upregulated fatty acid metabolism, stimulation decreased levels of acetylcarnitine (C2, Fig 8A) and small chain acylcarnitine (C4/Ci4 and C6-DC/C8-OH, Fig 8B - C) species, while the levels of medium-chain acylcarnitine species (C10, C14.1, and C18.3) were increased (Fig 8D - F). For the 10Hz stimulation only, we found an increase in the long-chain acylcarnitine species (C22, C22.1 and C22.2) (Fig 8G - I), indicating increased longer-chain fatty acid metabolism. In addition to upregulated fatty acid oxidation, increase in amino acid catabolism is linked to increase in C3, C4/Ci4 and C5 acylcarnitine species.Therefore, we next determined if changes in intracellular amino acids concentrations occurred with electrical stimulation and found significant increases in 6 amino acids, namely the branch chain amino acids valine and leucine/isoleucine, methionine, proline, ornithine and citrulline (Fig S3, Supplementary table 4). Together, these results demonstrated that electrical stimulation of myobundles yields a shift toward fatty acid oxidation and increased production of several intracellular amino acids.

Discussion

In this study, we investigated the effects of chronic intermittent electrical stimulation at 2 different frequencies on human engineered muscle structure, function and metabolism. Consistent with previous studies in engineered rodent muscles from primary and immortalized cells [37–41, 63], we found that electrical stimulation of human myobundles increased their absolute force production by 3-fold. The reproducibility and robustness of this result was confirmed in myobundles generated from multiple donors of different age and sex. In addition to contractile force, electrical stimulation increased myobundle size, myotube diameter and length, as well as glucose and fatty acid metabolic flux, independent of stimulation frequency. We also found frequency-dependent (10Hz vs. 1Hz) increase in myotube hypertrophy, speed of twitch relaxation and metabolism of longer chain fatty acids.

The role of functional innervation in inducing and maintaining adult myofiber size and function is well established with denervated human myofibers showing diameters and specific forces more than 50-fold smaller than innervated myofibers [21, 28, 64–70]. In our study, electrical stimulation increased specific force of human myobundles by 2-fold (Fig 5E) yielding the highest specific force reported for human engineered muscle (19.3

± 0.63mN/mm^2), but still significantly lower than those of native human skeletal muscles (150 – 250mN/mm^2) [21, 68]. Similarly, despite a 30–40% increase, myotube diameter (to 14.4 ± 0.2μm) remained small, in the size range of long-term denervated myofibers [28, 64, 66]. This result after only 7-day stimulation is expected, given that muscle development takes several months and that recovery of long-term denervated myofiber size to normal values by electrical stimulation requires 6 – 24 months [28, 64, 66]. On the other hand, long-term *in vitro* electrical stimulation could result in cell damage due to induction of electrochemical imbalance [71] and reactive oxygen species [72, 73], which could be minimized by use of appropriate carbon electrodes [73, 74] to apply bipolar, constant current stimuli [71] with optimized amplitude and duration [37, 40]. Even if non-damaging to cells, long-term stimulation of avascular myobundles would likely increase muscle size and metabolic demand to yield hypoxic stress, cell death, and formation of necrotic core [8, 13], which could be countered by applying oxygen carriers [75], perfusion bioreactors [76–78], or altered tissue geometry [13, 79, 80]. Nevertheless, long-term electrical stimulation alone may not permit complete engineered muscle maturation and additional neurotrophic factors [18], hormones [81], cells [82], and mechanical loading regimes [83] may be required to achieve adult myofiber size and force generating capacity *in vitro*.

Skeletal muscle hypertrophy occurs through two mechanisms: 1) increased satellite cell activation, proliferation and fusion into pre-existing or new myofibers and; 2) increased net protein synthesis in mature myofibers [11]. We found that electrical stimulation increased both nuclei number (Fig 1C) and myofiber size suggesting increased satellite cell or myoblast proliferation, which we [9] and others [38, 84] have previously reported in rodent engineered muscles. Furthermore, a single bout of exercise in native rodent and human skeletal muscle has been shown to increase mTORC1 activity that correlates with increased muscle mass [55, 57], while inhibition of mTORC1 prevented muscle hypertrophy [58]. Activation of mTORC1 increases protein synthesis through 4E-BP1 and S6K phosphorylation-dependent increase in translation initiation, elongation and ribosome biogenesis [85, 86]. Additionally, Akt and ERK1/2 activation are required for maximal mTORC1 activity through phosphorylation of TSC2 and consequent increased Rheb and mTORC1 interaction [59, 87]. In the present study, we found that electrical stimulation increased phosphorylation of S6K, Akt, mTOR, and ERK1/2 immediately following a bout of exercise (Fig 4A and B), suggesting increased activation of both mTORC1 and 2 complexes as previously reported in electrically stimulated human myotube cultures [88, 89]. Notably, greater increases in phosphorylation of these proteins at 10Hz vs. 1Hz stimulation, suggested that the frequency-dependent myofiber hypertrophy (Fig 2B and C) was a result of increased anabolic signaling. Additionally, stimulation-dependent increase in branch chain amino acid (BCAA) concentration (Fig S3A and B) was consistent with known regulatory roles of BCAA availability in mTORC1 activation and muscle hypertrophy found in resistance exercise [87, 90–94]. Despite greater increase in anabolic signaling (Fig 4) and myotube diameter (Fig 2B) with 10Hz vs. 1 Hz stimulation, both stimulation protocols induced similar increase in myobundle and F-actin areas (Fig 1D and E) and force generation (Fig 5). Recent studies have shown that human muscle hypertrophy and strength are similarly increased during low-load, high-repetition and high-load, low-repetition exercises until their total works are matched [95, 96] and/or exercise is performed to failure

[97, 98]. While each myobundle contraction at 10Hz stimulation produced higher force, the total number of contractions was higher at 1 Hz stimulation (Fig S1E), which resulted in similar total muscle activities likely yielding similar muscle growths. Additionally, exercise-induced muscle hypertrophy *in vivo* is often supported with increased capillary numbers and nutrient supply [99, 100], the absence of which in avascular myobundles may eventually limit the resulting tissue growth.

The electrical stimulation protocols used in our study did not induce mitochondrial biogenesis or glucose transporter upregulation (Fig 7E and F), unlike other studies utilizing 2 week chronic (24hrs/day) chronic electrical stimulation regimes [38, 39]. A likely difference is that our protocol did not induce metabolic stress as evidenced by the lack of AMPK phosphorylation (Fig 5A and B) [62]. The increase in sarcomeric but not metabolic proteins in stimulated myobundles was a likely reason for their increased fatigability, although the potentially role of oxygen diffusion limit due to increased myobundle size cannot be ruled out. The intermittent electrical stimulation used here mimics neural firing pattern of fast fibers and the increased fatigability could also signal a shift toward a fast-fiber phenotype [33, 34]. Only with higher frequency electrical stimulation did we find shorter half-relaxation times (Fig 6E) and increased expression of fast SERCA and CSQ isoforms, indicative of a partial fast-fiber type shift (Fig 6G). A more complete shift to a fast fiber phenotype may require increases in media glucose concentration [101] and longer culture times and higher stimulation frequencies (>40Hz) as required for full fiber-type shifts *in vivo* [32–34].

A classical feature of increased muscle activity is an increase in metabolic flux and a shift toward fatty acid substrate utilization [102]. Here, we found that electrical stimulation increased both glycolytic flux (Fig 7 C and D) and fatty acid oxidation. Specifically, independent of electrical stimulation frequency, we found a decrease in short-chain acylcarnitine species and an increase in medium acylcarnitines as recently reported in human subjects following exercise [49, 103, 104]. Furthermore, with higher frequency electrical stimulation we found increased abundance of long-chain acylcarnitines, which increase with exercise intensity in humans [105]. The changes in acylcarnitine species profile are indicative of increased fatty acid oxidation and increased longer chain fatty acid metabolism which occurs with developmental maturation and limited glucose availability [102, 106, 107].

Importantly, the increased myotube size, abundance of cross-striations, and muscle function all indicate a shift toward a more developmentally mature model of skeletal muscle. For increased physiological relevance, the human myobundles should accurately replicate structural and functional features of native adult skeletal muscle. For example, dystrophin is a cytoskeletal protein that functions in skeletal muscle to stabilize the plasma membrane and its mutations can result in the lethal Duchenne and Becker muscular dystrophies [108, 109]. Traditionally, *in vitro* 2D culture systems on both rigid tissue culture plastic and soft substrates show a primarily cytoplasmic localization of dystrophin [51, 52, 110]. Here we report for the first time a correct membrane localization of dystrophin in an *in vitro* primary muscle culture system, which we have previously observed in human iPSC-derived myobundles [20]. These findings suggest that our 3D myobundle system is a superior

biomimetic muscle equivalent compared to traditional 2D culture. Furthermore, we show that electrical stimulation can be used to increase dystrophin protein content without affecting mature membrane localization (Fig 3D and E). As such, we believe that human myobundles could be developed into an attractive *in vitro* system for studying human myopathies including Duchenne and Becker muscular dystrophy.

In summary, we have shown that electrical stimulation can promote engineered human muscle hypertrophy, structural organization, myotube maturation, force generation, and metabolic flux. Higher frequency stimulation yielded larger myotube size suggesting that further *in vitro* human myogenic maturation may be induced by stimulation patterns mimetic of *in vivo* muscle activity. The approach described here is a step towards engineering high-fidelity organ-on-a-chip models for studying human muscle biology and disease and discovering new therapeutics.

Supplementary Material

Refer to Web version on PubMed Central for supplementary material.

Acknowledgements

This work was supported by the NIH Grants AR070543 and AR065873 from National Institute of Arthritis and Musculoskeletal and Skin Disease (NIAMS) and grants UH3TR000505 and UG3TR002142 from the NIH Common Fund for the Microphysiological Systems Initiative and NIAMS. The content of the manuscript is solely the responsibility of the authors and does not necessarily represent the official views of the funding agencies.

References

[1]. Alway SE, Myers MJ, Mohamed JS, Regulation of satellite cell function in sarcopenia, Front Aging Neurosci 6 (2014) 246. [PubMed: 25295003]

[2]. Doherty TJ, Invited review: Aging and sarcopenia, J Appl Physiol (1985) 95(4) (2003) 1717–27. [PubMed: 12970377]

[3]. Laing NG, Genetics of neuromuscular disorders, Crit Rev Clin Lab Sci 49(2) (2012) 33–48. [PubMed: 22468856]

[4]. Baskin KK, Winders BR, Olson EN, Muscle as a “mediator” of systemic metabolism, Cell Metab 21(2) (2015) 237–48. [PubMed: 25651178]

[5]. Cheng CS, Davis BN, Madden L, Bursac N, Truskey GA, Physiology and metabolism of tissue-engineered skeletal muscle, Exp Biol Med (Maywood) 239(9) (2014) 1203–14. [PubMed: 24912506]

[6]. Hay M, Thomas DW, Craighead JL, Economides C, Rosenthal J, Clinical development success rates for investigational drugs, Nat Biotechnol 32(1) (2014) 40–51. [PubMed: 24406927]

[7]. Bursac N, Juhas M, Rando TA, Synergizing Engineering and Biology to Treat and Model Skeletal Muscle Injury and Disease, Annu Rev Biomed Eng 17 (2015) 217–42. [PubMed: 26643021]

[8]. Juhas M, Bursac N, Roles of adherent myogenic cells and dynamic culture in engineered muscle function and maintenance of satellite cells, Biomaterials 35(35) (2014) 9438–46. [PubMed: 25154662]

[9]. Juhas M, Engelmayr GC, Jr., Fontanella AN, Palmer GM, Bursac N, Biomimetic engineered muscle with capacity for vascular integration and functional maturation in vivo, Proc Natl Acad Sci U S A 111(15) (2014) 5508–13. [PubMed: 24706792]

[10]. Khodabukus A, Baar K, Factors That Affect Tissue-Engineered Skeletal Muscle Function and Physiology, Cells Tissues Organs 202(3–4) (2016) 159–168. [PubMed: 27825147]

[11]. Shadrin IY, Khodabukus A, Bursac N, Striated muscle function, regeneration, and repair, Cell Mol Life Sci 73(22) (2016) 4175–4202. [PubMed: 27271751]

[12]. Juhas M, Ye J, Bursac N, Design, evaluation, and application of engineered skeletal muscle, Methods 99 (2016) 81–90. [PubMed: 26455485]

[13]. Khodabukus A, Prabhu N, Wang J, Bursac N, In Vitro Tissue-Engineered Skeletal Muscle Models for Studying Muscle Physiology and Disease, Adv Healthc Mater (2018) e1701498. [PubMed: 29696831]

[14]. Khodabukus A, Paxton JZ, Donnelly K, Baar K, Engineered muscle: a tool for studying muscle physiology and function, Exerc Sport Sci Rev 35(4) (2007) 186–91. [PubMed: 17921787]

[15]. Martin NR, Passey SL, Player DJ, Khodabukus A, Ferguson RA, Sharples AP, Mudera V, Baar K, Lewis MP, Factors affecting the structure and maturation of human tissue engineered skeletal muscle, Biomaterials 34(23) (2013) 5759–65. [PubMed: 23643182]

[16]. Bian W, Liau B, Badie N, Bursac N, Mesoscopic hydrogel molding to control the 3D geometry of bioartificial muscle tissues, Nat Protoc 4(10) (2009) 1522–34. [PubMed: 19798085]

[17]. Hinds S, Bian W, Dennis RG, Bursac N, The role of extracellular matrix composition in structure and function of bioengineered skeletal muscle, Biomaterials 32(14) (2011) 3575–83. [PubMed: 21324402]

[18]. Bian W, Bursac N, Soluble miniagrin enhances contractile function of engineered skeletal muscle, FASEB J 26(2) (2012) 955–65. [PubMed: 22075647]

[19]. Madden L, Juhas M, Kraus WE, Truskey GA, Bursac N, Bioengineered human myobundles mimic clinical responses of skeletal muscle to drugs, Elife 4 (2015) e04885. [PubMed: 25575180]

[20]. Rao L, Qian Y, Khodabukus A, Ribar T, Bursac N, Engineering human pluripotent stem cells into a functional skeletal muscle tissue, Nat Commun 9(1) (2018) 126. [PubMed: 29317646]

[21]. Roche SM, Gumucio JP, Brooks SV, Mendias CL, Claflin DR, Measurement of Maximum Isometric Force Generated by Permeabilized Skeletal Muscle Fibers, J Vis Exp (100) (2015) e52695. [PubMed: 26131687]

[22]. Ashby PR, Pincon-Raymond M, Harris AJ, Regulation of myogenesis in paralyzed muscles in the mouse mutants peroneal muscular atrophy and muscular dysgenesis, Dev Biol 156(2) (1993) 529–36. [PubMed: 8462749]

[23]. Harris AJ, Fitzsimons RB, McEwan JC, Neural control of the sequence of expression of myosin heavy chain isoforms in foetal mammalian muscles, Development 107(4) (1989) 751–69. [PubMed: 2534377]

[24]. Ross JJ, Duxson MJ, Harris AJ, Neural determination of muscle fibre numbers in embryonic rat lumbrical muscles, Development 100(3) (1987) 395–409. [PubMed: 3652977]

[25]. DiMario JX, Stockdale FE, Both myoblast lineage and innervation determine fiber type and are required for expression of the slow myosin heavy chain 2 gene, Dev Biol 188(1) (1997) 167–80. [PubMed: 9245520]

[26]. Midrio M, The denervated muscle: facts and hypotheses. A historical review, Eur J Appl Physiol 98(1) (2006) 1–21. [PubMed: 16896733]

[27]. Carraro U, Boncompagni S, Gobbo V, Rossini K, Zampieri S, Mosole S, Ravara B, Nori A, Stramare R, Ambrosio F, Piccione F, Masiero S, Vindigni V, Gargiulo P, Protasi F, Kern H, Pond A, Marcante A, Persistent Muscle Fiber Regeneration in Long Term Denervation. Past, Present, Future, Eur J Transl Myol 25(2) (2015) 4832. [PubMed: 26913148]

[28]. Kern H, Boncompagni S, Rossini K, Mayr W, Fano G, Zanin ME, Podhorska-Okolow M, Protasi F, Carraro U, Long-term denervation in humans causes degeneration of both contractile and excitation-contraction coupling apparatus, which is reversible by functional electrical stimulation (FES): a role for myofiber regeneration?, J Neuropathol Exp Neurol 63(9) (2004) 919–31. [PubMed: 15453091]

[29]. Salmons S, Sreter FA, Significance of impulse activity in the transformation of skeletal muscle type, Nature 263(5572) (1976) 30–4. [PubMed: 958462]

[30]. Eken T, Elder GC, Lomo T, Development of tonic firing behavior in rat soleus muscle, J Neurophysiol 99(4) (2008) 1899–905. [PubMed: 18256168]

[31]. Windisch A, Gundersen K, Szabolcs MJ, Gruber H, Lomo T, Fast to slow transformation of denervated and electrically stimulated rat muscle, J Physiol 510 (Pt 2) (1998) 623–32. [PubMed: 9706009]

[32]. Gorza L, Gundersen K, Lomo T, Schiaffino S, Westgaard RH, Slow-to-fast transformation of denervated soleus muscles by chronic high-frequency stimulation in the rat, J Physiol 402 (1988) 627–49. [PubMed: 3236251]

[33]. Westgaard RH, Lomo T, Control of contractile properties within adaptive ranges by patterns of impulse activity in the rat, J Neurosci 8(12) (1988) 4415–26. [PubMed: 3199182]

[34]. Hennig R, Lomo T, Firing patterns of motor units in normal rats, Nature 314(6007) (1985) 164–6. [PubMed: 3974720]

[35]. Nikolic N, Bakke SS, Kase ET, Rudberg I, Flo Halle I, Rustan AC, Thoresen GH, Aas V, Electrical pulse stimulation of cultured human skeletal muscle cells as an in vitro model of exercise, PLoS One 7(3) (2012) e33203. [PubMed: 22457744]

[36]. Tarum J, Folkesson M, Atherton PJ, Kadi F, Electrical pulse stimulation: an in vitro exercise model for the induction of human skeletal muscle cell hypertrophy. A proof-of-concept study, Exp Physiol 102(11) (2017) 1405–1413. [PubMed: 28861930]

[37]. Donnelly K, Khodabukus A, Philp A, Deldicque L, Dennis RG, Baar K, A novel bioreactor for stimulating skeletal muscle in vitro, Tissue Eng Part C Methods 16(4) (2010) 711–8. [PubMed: 19807268]

[38]. Khodabukus A, Baehr LM, Bodine SC, Baar K, Role of contraction duration in inducing fast-to-slow contractile and metabolic protein and functional changes in engineered muscle, J Cell Physiol 230(10) (2015) 2489–97. [PubMed: 25857846]

[39]. Khodabukus A, Baar K, Streptomycin decreases the functional shift to a slow phenotype induced by electrical stimulation in engineered muscle, Tissue Eng Part A 21(5–6) (2015) 1003–12. [PubMed: 25333771]

[40]. Khodabukus A, Baar K, Defined electrical stimulation emphasizing excitability for the development and testing of engineered skeletal muscle, Tissue Eng Part C Methods 18(5) (2012) 349–57. [PubMed: 22092374]

[41]. Huang YC, Dennis RG, Baar K, Cultured slow vs. fast skeletal muscle cells differ in physiology and responsiveness to stimulation, Am J Physiol Cell Physiol 291(1) (2006) C11–7. [PubMed: 16436474]

[42]. Liao IC, Liu JB, Bursac N, Leong KW, Effect of Electromechanical Stimulation on the Maturation of Myotubes on Aligned Electrospun Fibers, Cell Mol Bioeng 1(2–3) (2008) 133–145. [PubMed: 19774099]

[43]. Jackman CP, Carlson AL, Bursac N, Dynamic culture yields engineered myocardium with near-adult functional output, Biomaterials 111 (2016) 66–79. [PubMed: 27723557]

[44]. Khodabukus A, Baar K, Regulating Fibrinolysis to Engineer Skeletal Muscle from the C2C12 Cell Line, Tissue Eng Part C Methods (2009).

[45]. Nedachi T, Fujita H, Kanzaki M, Contractile C2C12 myotube model for studying exercise-inducible responses in skeletal muscle, Am J Physiol Endocrinol Metab 295(5) (2008) E1191–204. [PubMed: 18780777]

[46]. Fujita H, Nedachi T, Kanzaki M, Accelerated de novo sarcomere assembly by electric pulse stimulation in C2C12 myotubes, Exp Cell Res 313(9) (2007) 1853–65. [PubMed: 17425954]

[47]. Khodabukus A, Baar K, Contractile and metabolic properties of engineered skeletal muscle derived from slow and fast phenotype mouse muscle, J Cell Physiol 230(8) (2015) 1750–7. [PubMed: 25335966]

[48]. Khodabukus A, Baar K, The effect of serum origin on tissue engineered skeletal muscle function, J Cell Biochem 115(12) (2014) 2198–207. [PubMed: 25146978]

[49]. Huffman KM, Koves TR, Hubal MJ, Abouassi H, Beri N, Bateman LA, Stevens RD, Ilkayeva OR, Hoffman EP, Muoio DM, Kraus WE, Metabolite signatures of exercise training in human skeletal muscle relate to mitochondrial remodelling and cardiometabolic fitness, Diabetologia 57(11) (2014) 2282–95. [PubMed: 25091629]

[50]. Koves TR, Ussher JR, Noland RC, Slentz D, Mosedale M, Ilkayeva O, Bain J, Stevens R, Dyck JR, Newgard CB, Lopaschuk GD, Muoio DM, Mitochondrial overload and incomplete fatty acid oxidation contribute to skeletal muscle insulin resistance, Cell Metab 7(1) (2008) 45–56. [PubMed: 18177724]

[51]. Serena E, Zatti S, Zoso A, Lo Verso F, Tedesco FS, Cossu G, Elvassore N, Skeletal Muscle Differentiation on a Chip Shows Human Donor Mesoangioblasts' Efficiency in Restoring Dystrophin in a Duchenne Muscular Dystrophy Model, Stem Cells Transl Med 5(12) (2016) 1676–1683. [PubMed: 27502519]

[52]. Welch EM, Barton ER, Zhuo J, Tomizawa Y, Friesen WJ, Trifillis P, Paushkin S, Patel M, Trotta CR, Hwang S, Wilde RG, Karp G, Takasugi J, Chen G, Jones S, Ren H, Moon YC, Corson D, Turpoff AA, Campbell JA, Conn MM, Khan A, Almstead NG, Hedrick J, Mollin A, Risher N, Weetall M, Yeh S, Branstrom AA, Colacino JM, Babiak J, Ju WD, Hirawat S, Northcutt VJ, Miller LL, Spatrick P, He F, Kawana M, Feng H, Jacobson A, Peltz SW, Sweeney HL, PTC124 targets genetic disorders caused by nonsense mutations, Nature 447(7140) (2007) 87–91. [PubMed: 17450125]

[53]. Sarbassov DD, Ali SM, Kim DH, Guertin DA, Latek RR, Erdjument-Bromage H, Tempst P, Sabatini DM, Rictor, a novel binding partner of mTOR, defines a rapamycin-insensitive and raptor-independent pathway that regulates the cytoskeleton, Curr Biol 14(14) (2004) 1296–302. [PubMed: 15268862]

[54]. Marcotte GR, West DW, Baar K, The molecular basis for load-induced skeletal muscle hypertrophy, Calcif Tissue Int 96(3) (2015) 196–210. [PubMed: 25359125]

[55]. Baar K, Esser K, Phosphorylation of p70(S6k) correlates with increased skeletal muscle mass following resistance exercise, Am J Physiol 276(1 Pt 1) (1999) C120–7. [PubMed: 9886927]

[56]. Drummond MJ, Fry CS, Glynn EL, Dreyer HC, Dhanani S, Timmerman KL, Volpi E, Rasmussen BB, Rapamycin administration in humans blocks the contraction-induced increase in skeletal muscle protein synthesis, J Physiol 587(Pt 7) (2009) 1535–46. [PubMed: 19188252]

[57]. Terzis G, Georgiadis G, Stratakos G, Vogiatzis I, Kavouras S, Manta P, Mascher H, Blomstrand E, Resistance exercise-induced increase in muscle mass correlates with p70S6 kinase phosphorylation in human subjects, Eur J Appl Physiol 102(2) (2008) 145–52. [PubMed: 17874120]

[58]. Bodine SC, Stitt TN, Gonzalez M, Kline WO, Stover GL, Bauerlein R, Zlotchenko E, Scrimgeour A, Lawrence JC, Glass DJ, Yancopoulos GD, Akt/mTOR pathway is a crucial regulator of skeletal muscle hypertrophy and can prevent muscle atrophy in vivo, Nat Cell Biol 3(11) (2001) 1014–9. [PubMed: 11715023]

[59]. Winter JN, Jefferson LS, Kimball SR, ERK and Akt signaling pathways function through parallel mechanisms to promote mTORC1 signaling, Am J Physiol Cell Physiol 300(5) (2011) C1172–80. [PubMed: 21289294]

[60]. Guertin DA, Stevens DM, Thoreen CC, Burds AA, Kalaany NY, Moffat J, Brown M, Fitzgerald KJ, Sabatini DM, Ablation in mice of the mTORC components raptor, rictor, or mLST8 reveals that mTORC2 is required for signaling to Akt-FOXO and PKCalpha, but not S6K1, Dev Cell 11(6) (2006) 859–71. [PubMed: 17141160]

[61]. Sarbassov DD, Guertin DA, Ali SM, Sabatini DM, Phosphorylation and regulation of Akt/PKB by the rictor-mTOR complex, Science 307(5712) (2005) 1098–101. [PubMed: 15718470]

[62]. Hardie DG, AMP-activated protein kinase: an energy sensor that regulates all aspects of cell function, Genes Dev 25(18) (2011) 1895–908. [PubMed: 21937710]

[63]. Ito A, Yamamoto Y, Sato M, Ikeda K, Yamamoto M, Fujita H, Nagamori E, Kawabe Y, Kamihira M, Induction of functional tissue-engineered skeletal muscle constructs by defined electrical stimulation, Sci Rep 4 (2014) 4781. [PubMed: 24759171]

[64]. Boncompagni S, Kern H, Rossini K, Hofer C, Mayr W, Carraro U, Protasi F, Structural differentiation of skeletal muscle fibers in the absence of innervation in humans, Proc Natl Acad Sci U S A 104(49) (2007) 19339–44. [PubMed: 18042706]

[65]. Dow DE, Cederna PS, Hassett CA, Kostrominova TY, Faulkner JA, Dennis RG, Number of contractions to maintain mass and force of a denervated rat muscle, Muscle Nerve 30(1) (2004) 77–86. [PubMed: 15221882]

[66]. Modlin M, Forstner C, Hofer C, Mayr W, Richter W, Carraro U, Protasi F, Kern H, Electrical stimulation of denervated muscles: first results of a clinical study, Artif Organs 29(3) (2005) 203–6. [PubMed: 15725217]

[67]. Akagi R, Takai Y, Ohta M, Kanehisa H, Kawakami Y, Fukunaga T, Muscle volume compared to cross-sectional area is more appropriate for evaluating muscle strength in young and elderly individuals, Age Ageing 38(5) (2009) 564–9. [PubMed: 19596739]

[68]. Krivickas LS, Dorer DJ, Ochala J, Frontera WR, Relationship between force and size in human single muscle fibres, Exp Physiol 96(5) (2011) 539–47. [PubMed: 21317219]

[69]. Urbanchek MG, Picken EB, Kalliainen LK, Kuzon WM, Jr., Specific force deficit in skeletal muscles of old rats is partially explained by the existence of denervated muscle fibers, J Gerontol A Biol Sci Med Sci 56(5) (2001) B191–7. [PubMed: 11320099]

[70]. Carlson BM, Billington L, Faulkner J, Studies on the regenerative recovery of long-term denervated muscle in rats, Restor Neurol Neurosci 10(2) (1996) 77–84. [PubMed: 21551856]

[71]. Scheiner A, Mortimer JT, Roessmann U, Imbalanced biphasic electrical stimulation: muscle tissue damage, Ann Biomed Eng 18(4) (1990) 407–25. [PubMed: 2221508]

[72]. Diaz-Vegas A, Campos CA, Contreras-Ferrat A, Casas M, Buvinic S, Jaimovich E, Espinosa A, ROS Production via P2Y1-PKC-NOX2 Is Triggered by Extracellular ATP after Electrical Stimulation of Skeletal Muscle Cells, PLoS One 10(6) (2015) e0129882. [PubMed: 26053483]

[73]. Serena E, Figallo E, Tandon N, Cannizzaro C, Gerecht S, Elvassore N, Vunjak-Novakovic G, Electrical stimulation of human embryonic stem cells: cardiac differentiation and the generation of reactive oxygen species, Exp Cell Res 315(20) (2009) 3611–9. [PubMed: 19720058]

[74]. Tandon N, Marsano A, Maidhof R, Wan L, Park H, Vunjak-Novakovic G, Optimization of electrical stimulation parameters for cardiac tissue engineering, J Tissue Eng Regen Med 5(6) (2011) e115–25. [PubMed: 21604379]

[75]. Radisic M, Park H, Chen F, Salazar-Lazzaro JE, Wang Y, Dennis R, Langer R, Freed LE, Vunjak-Novakovic G, Biomimetic approach to cardiac tissue engineering: oxygen carriers and channeled scaffolds, Tissue Eng 12(8) (2006) 2077–91. [PubMed: 16968150]

[76]. Skardal A, Murphy SV, Devarasetty M, Mead I, Kang HW, Seol YJ, Shrike Zhang Y, Shin SR, Zhao L, Aleman J, Hall AR, Shupe TD, Kleensang A, Dokmeci MR, Jin Lee S, Jackson JD, Yoo JJ, Hartung T, Khademhosseini A, Soker S, Bishop CE, Atala A, Multi-tissue interactions in an integrated three-tissue organ-on-a-chip platform, Sci Rep 7(1) (2017) 8837. [PubMed: 28821762]

[77]. Vernetti L, Gough A, Baetz N, Blutt S, Broughman JR, Brown JA, Foulke-Abel J, Hasan N, In J, Kelly E, Kovbasnjuk O, Repper J, Senutovitch N, Stabb J, Yeung C, Zachos NC, Donowitz M, Estes M, Himmelfarb J, Truskey G, Wikswo JP, Taylor DL, Functional Coupling of Human Microphysiology Systems: Intestine, Liver, Kidney Proximal Tubule, Blood-Brain Barrier and Skeletal Muscle, Sci Rep 7 (2017) 42296. [PubMed: 28176881]

[78]. Rangarajan S, Madden L, Bursac N, Use of flow, electrical, and mechanical stimulation to promote engineering of striated muscles, Ann Biomed Eng 42(7) (2014) 1391–405. [PubMed: 24366526]

[79]. Bian W, Juhas M, Pfeiler TW, Bursac N, Local tissue geometry determines contractile force generation of engineered muscle networks, Tissue Eng Part A 18(9–10) (2012) 957–67. [PubMed: 22115339]

[80]. Bian W, Bursac N, Engineered skeletal muscle tissue networks with controllable architecture, Biomaterials 30(7) (2009) 1401–12. [PubMed: 19070360]

[81]. Huang YC, Dennis RG, Larkin L, Baar K, Rapid formation of functional muscle in vitro using fibrin gels, J Appl Physiol 98(2) (2005) 706–13. [PubMed: 15475606]

[82]. Martin NR, Passey SL, Player DJ, Mudera V, Baar K, Greensmith L, Lewis MP, Neuromuscular Junction Formation in Tissue-Engineered Skeletal Muscle Augments Contractile Function and Improves Cytoskeletal Organization, Tissue Eng Part A 21(19–20) (2015) 2595–604. [PubMed: 26166548]

[83]. Powell CA, Smiley BL, Mills J, Vandenburgh HH, Mechanical stimulation improves tissue-engineered human skeletal muscle, Am J Physiol Cell Physiol 283(5) (2002) C1557–65. [PubMed: 12372817]

[84]. Ikeda K, Ito A, Sato M, Kawabe Y, Kamihira M, Improved contractile force generation of tissue-engineered skeletal muscle constructs by IGF-I and Bcl-2 gene transfer with electrical pulse stimulation, Regenerative Therapy 3 (2016) 38–44.

[85]. Marabita M, Baraldo M, Solagna F, Ceelen JJM, Sartori R, Nolte H, Nemazanyy I, Pyronnet S, Kruger M, Pende M, Blaauw B, S6K1 Is Required for Increasing Skeletal Muscle Force during Hypertrophy, Cell Rep 17(2) (2016) 501–513. [PubMed: 27705797]

[86]. Ma XM, Blenis J, Molecular mechanisms of mTOR-mediated translational control, Nat Rev Mol Cell Biol 10(5) (2009) 307–18. [PubMed: 19339977]

[87]. Goodman CA, Miu MH, Frey JW, Mabrey DM, Lincoln HC, Ge Y, Chen J, Hornberger TA, A PI3K/PKB-Independent Activation of mTOR Signaling Is Sufficient to Induce Skeletal Muscle Hypertrophy, Mol Biol Cell (2010).

[88]. Christensen CS, Christensen DP, Lundh M, Dahllof MS, Haase TN, Velasquez JM, Laye MJ, Mandrup-Poulsen T, Solomon TP, Skeletal Muscle to Pancreatic beta-Cell Cross-talk: The Effect of Humoral Mediators Liberated by Muscle Contraction and Acute Exercise on beta-Cell Apoptosis, J Clin Endocrinol Metab 100(10) (2015) E1289–98. [PubMed: 26218753]

[89]. Scheler M, Irmler M, Lehr S, Hartwig S, Staiger H, Al-Hasani H, Beckers J, de Angelis MH, Haring HU, Weigert C, Cytokine response of primary human myotubes in an in vitro exercise model, Am J Physiol Cell Physiol 305(8) (2013) C877–86. [PubMed: 23926130]

[90]. O'Neil TK, Duffy LR, Frey JW, Hornberger TA, The role of phosphoinositide 3-kinase and phosphatidic acid in the regulation of mammalian target of rapamycin following eccentric contractions, J Physiol 587(Pt 14) (2009) 3691–701. [PubMed: 19470781]

[91]. Hornberger TA, Chu WK, Mak YW, Hsiung JW, Huang SA, Chien S, The role of phospholipase D and phosphatidic acid in the mechanical activation of mTOR signaling in skeletal muscle, Proc Natl Acad Sci U S A 103(12) (2006) 4741–6. [PubMed: 16537399]

[92]. Sancak Y, Peterson TR, Shaul YD, Lindquist RA, Thoreen CC, Bar-Peled L, Sabatini DM, The Rag GTPases bind raptor and mediate amino acid signaling to mTORC1, Science 320(5882) (2008) 1496–501. [PubMed: 18497260]

[93]. Drummond MJ, Fry CS, Glynn EL, Timmerman KL, Dickinson JM, Walker DK, Gundermann DM, Volpi E, Rasmussen BB, Skeletal muscle amino acid transporter expression is increased in young and older adults following resistance exercise, J Appl Physiol (1985) 111(1) (2011) 135–42. [PubMed: 21527663]

[94]. Biolo G, Maggi SP, Williams BD, Tipton KD, Wolfe RR, Increased rates of muscle protein turnover and amino acid transport after resistance exercise in humans, Am J Physiol 268(3 Pt 1) (1995) E514–20. [PubMed: 7900797]

[95]. Bemben DA, Fetters NL, Bemben MG, Nabavi N, Koh ET, Musculoskeletal responses to high- and low-intensity resistance training in early postmenopausal women, Med Sci Sports Exerc 32(11) (2000) 1949–57. [PubMed: 11079527]

[96]. Alegre LM, Aguado X, Rojas-Martin D, Martin-Garcia M, Ara I, Csapo R, Load-controlled moderate and high-intensity resistance training programs provoke similar strength gains in young women, Muscle Nerve 51(1) (2015) 92–101. [PubMed: 24828840]

[97]. Mitchell CJ, Churchward-Venne TA, West DW, Burd NA, Breen L, Baker SK, Phillips SM, Resistance exercise load does not determine training-mediated hypertrophic gains in young men, J Appl Physiol (1985) 113(1) (2012) 71–7. [PubMed: 22518835]

[98]. Burd NA, West DW, Staples AW, Atherton PJ, Baker JM, Moore DR, Holwerda AM, Parise G, Rennie MJ, Baker SK, Phillips SM, Low-load high volume resistance exercise stimulates muscle protein synthesis more than high-load low volume resistance exercise in young men, PLoS One 5(8) (2010) e12033. [PubMed: 20711498]

[99]. Green H, Goreham C, Ouyang J, Ball-Burnett M, Ranney D, Regulation of fiber size, oxidative potential, and capillarization in human muscle by resistance exercise, Am J Physiol 276(2 Pt 2) (1999) R591–6. [PubMed: 9950941]

[100]. McCall GE, Byrnes WC, Dickinson A, Pattany PM, Fleck SJ, Muscle fiber hypertrophy, hyperplasia, and capillary density in college men after resistance training, J Appl Physiol (1985) 81(5) (1996) 2004–12. [PubMed: 8941522]

[101]. Khodabukus A, Baar K, Glucose concentration and streptomycin alter in vitro muscle function and metabolism, J Cell Physiol 230(6) (2015) 1226–34. [PubMed: 25358470]

[102]. Henriksson J, Muscle fuel selection: effect of exercise and training, Proc Nutr Soc 54(1) (1995) 125–38. [PubMed: 7568247]

[103]. ter Veld F, Primassin S, Hoffmann L, Mayatepek E, Spiekerkoetter U, Corresponding increase in long-chain acyl-CoA and acylcarnitine after exercise in muscle from VLCAD mice, J Lipid Res 50(8) (2009) 1556–62. [PubMed: 18980943]

[104]. Zhang J, Light AR, Hoppel CL, Campbell C, Chandler CJ, Burnett DJ, Souza EC, Casazza GA, Hughen RW, Keim NL, Newman JW, Hunter GR, Fernandez JR, Garvey WT, Harper ME, Fiehn O, Adams SH, Acylcarnitines as markers of exercise-associated fuel partitioning, xenometabolism, and potential signals to muscle afferent neurons, Exp Physiol 102(1) (2017) 48–69. [PubMed: 27730694]

[105]. Hiatt WR, Regensteiner JG, Wolfel EE, Ruff L, Brass EP, Carnitine and acylcarnitine metabolism during exercise in humans. Dependence on skeletal muscle metabolic state, J Clin Invest 84(4) (1989) 1167–73. [PubMed: 2794054]

[106]. Challiss RA, Ferre P, Integration of carbohydrate and lipid metabolism in skeletal muscle during postnatal development, Reprod Nutr Dev 28(3B) (1988) 805–15. [PubMed: 3055103]

[107]. Carroll JE, Shumate JB, Villadiego A, Choksi RM, Morse DP, Skeletal muscle fatty acid oxidation during early postnatal development in the rat, Biol Neonate 43(3–4) (1983) 191–7. [PubMed: 6222770]

[108]. Hoffman EP, Brown RH, Jr., Kunkel LM, Dystrophin: the protein product of the Duchenne muscular dystrophy locus, Cell 51(6) (1987) 919–28. [PubMed: 3319190]

[109]. Campbell KP, Kahl SD, Association of dystrophin and an integral membrane glycoprotein, Nature 338(6212) (1989) 259–62. [PubMed: 2493582]

[110]. Zacharias U, Purfurst B, Schowel V, Morano I, Spuler S, Haase H, Ahnak1 abnormally localizes in muscular dystrophies and contributes to muscle vesicle release, J Muscle Res Cell Motil 32(4–5) (2011) 271–80. [PubMed: 22057634]

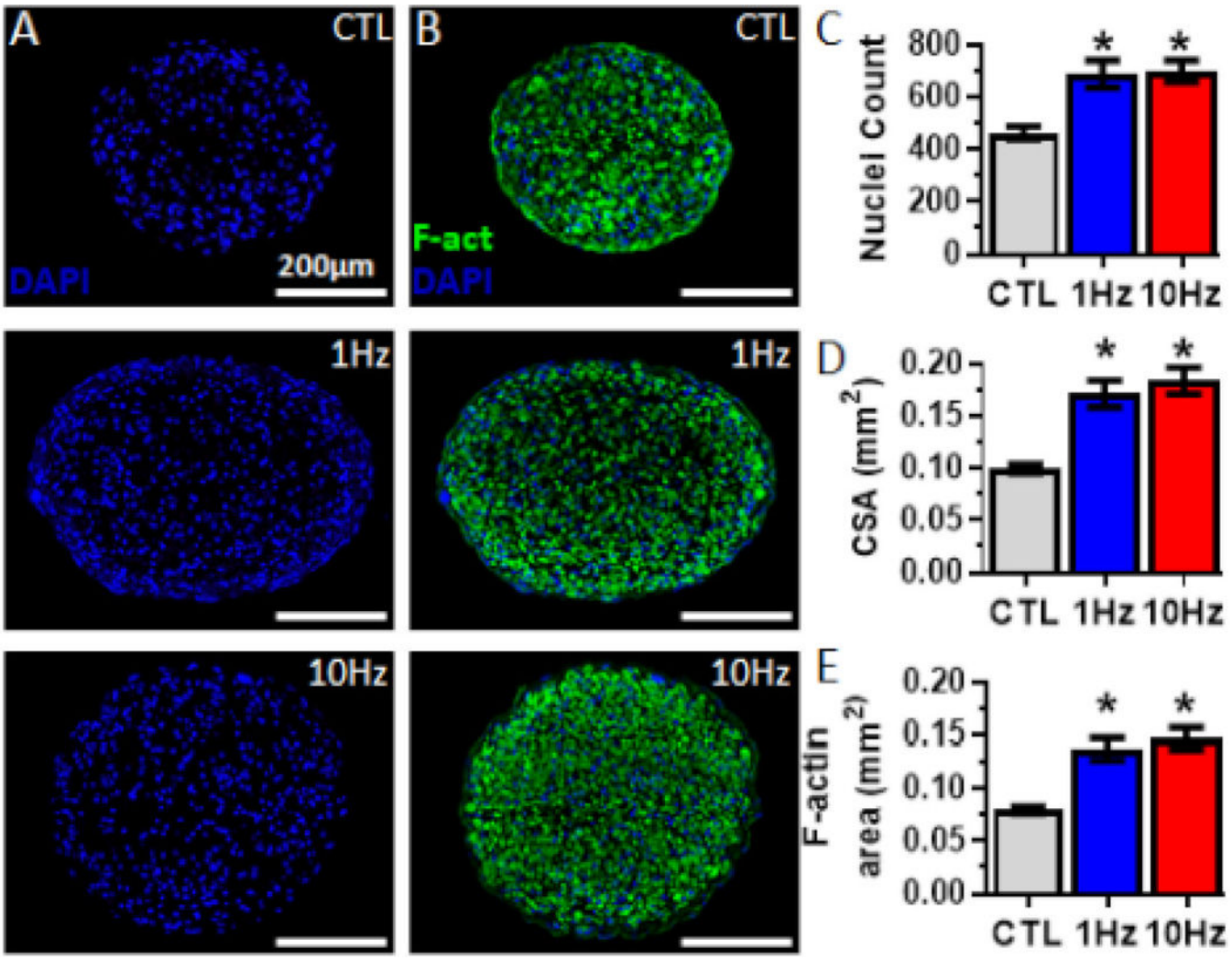

Figure 1. Effects of electrical stimulation on myobundle structure.

(A,B) Representative myobundle cross-sectional images stained for (**A**) nuclei (blue) and (**B**) filamentous actin (F-act, green) and nuclei in myobundles that were not stimulated (CTL) or electrically stimulated at 1 or 10Hz. (**C-E**) Quantification of number of (**C**) nuclei per cross-section, (**D**) myobundle cross-sectional area and (**E**) F-actin area (n = 16 myobundles from N = 4 donors per group). *, P<0.01 vs. CTL.

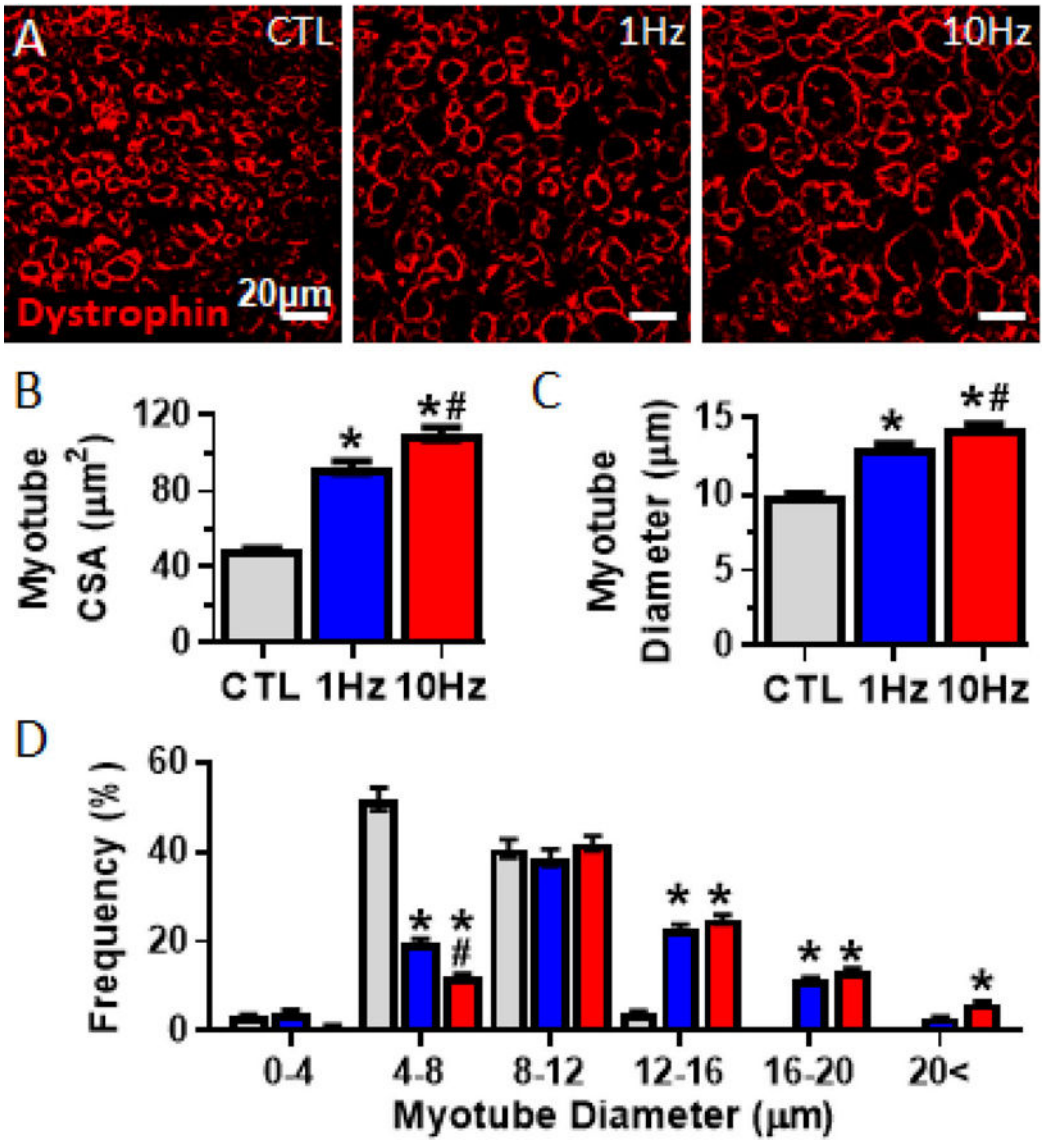

Figure 2. Effects of electrical stimulation on myotube size.

(**A**) Representative myobundle cross-sectional images stained for dystrophin (red). (**B, C**) Quantification of (**B**) myotube cross-sectional area and (**C**) myotube diameter. (**D**) Frequency histogram of myotube diameters (n = 500 myotubes from N = 4 donors per group). *, P<0.001 vs. CTL; # P<0.001 vs. 1Hz.

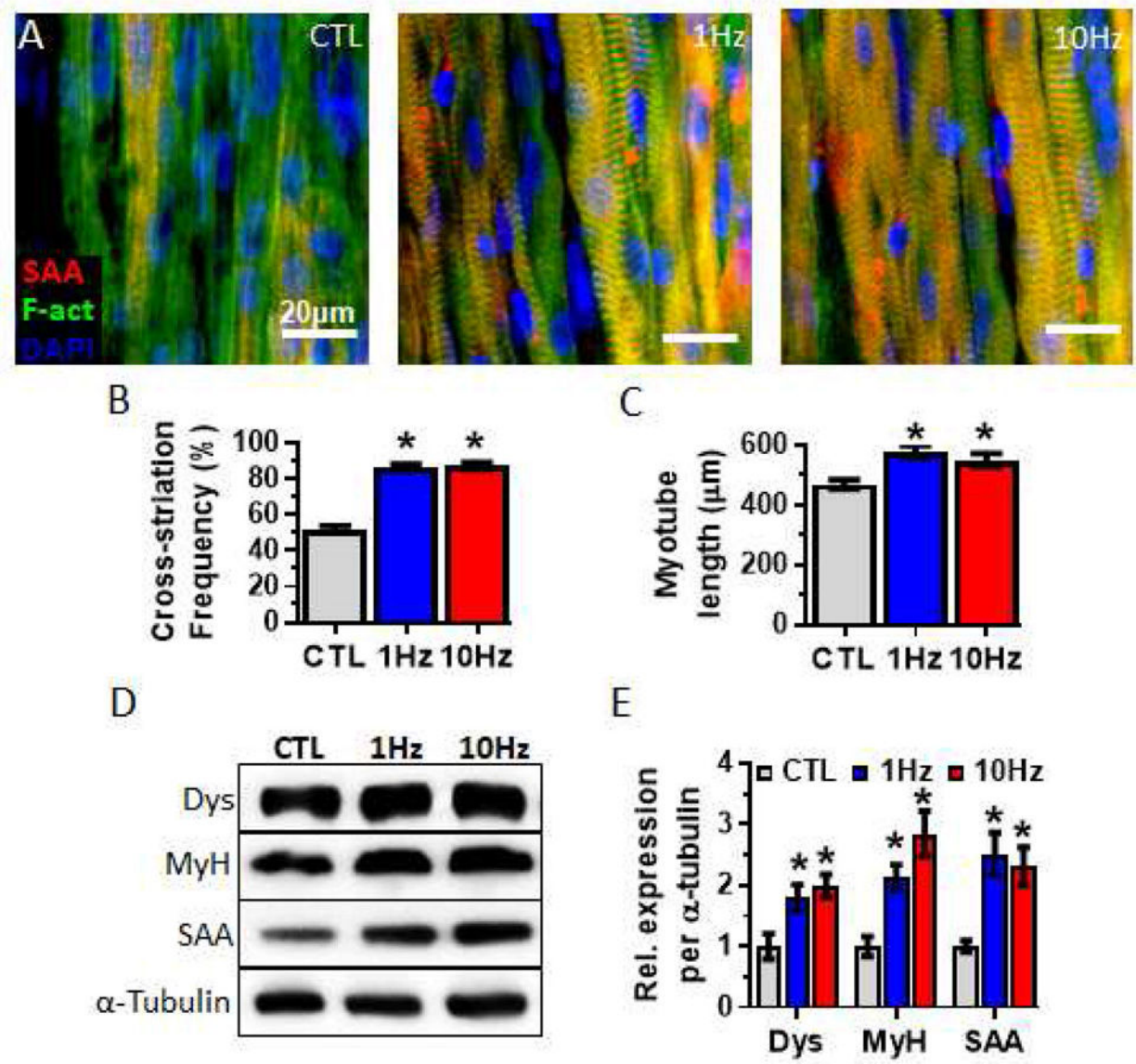

Figure 3. Effects of electrical stimulation on myotube structure and sarcomeric protein content.

(**A**) Representative images of whole myobundles stained for sarcomeric α-actinin (SAA, red), filamentous actin (F-act, green), and nuclei (blue). (**B, C**) Quantifications of (**B**) the percentage of cross-striated myotubes (n = 300 myotubes from N = 3 donors per group) and (**C**) myotube length (n =225 myotubes from N = 3 donors per group). (**D**) Representative western blots from a single donor showing expression of the sarcomeric proteins dystrophin (Dys), myosin heavy chain (MyH) and SAA, with α-tubulin serving as a protein loading control. (**E**) Quantifications of western blots averaged for 3 donors with protein abundance normalized to α-tubulin. *, P<0.05 vs. CTL.

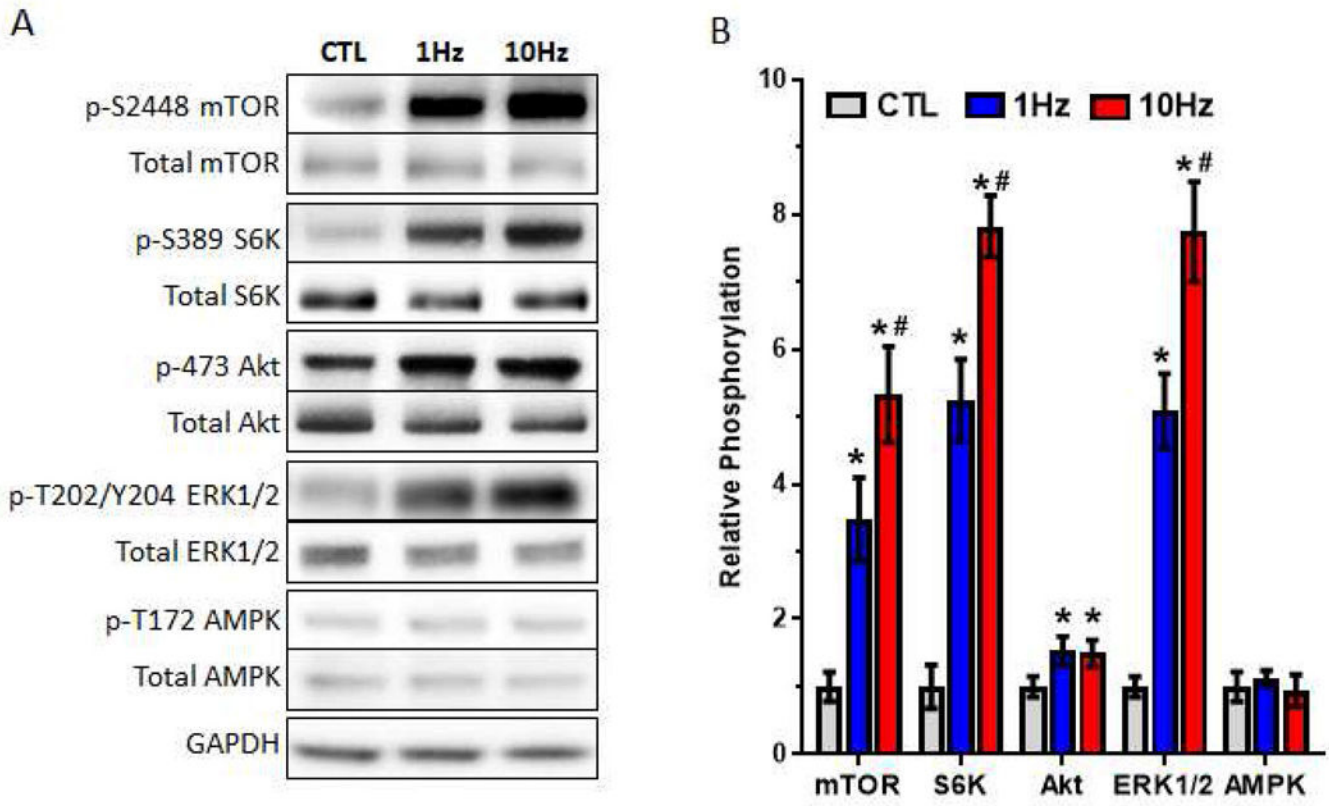

Figure 4. Effect of electrical stimulation on kinase phosphorylation changes in myobundles.

(**A**) Representative western blots for phosphorylated (Ser2448) and total mTOR, phosphorylated (Thr389) and total S6K, phosphorylated (Ser473) and total Akt, phosphorylated (Thr202/Tyr204) and total ERK1/2, phosphorylated (Thr172) and total AMPK, and GAPDH (loading control) immediately following the of last bout of electrical stimulation in two-week myobundles (**B**) Quantified ratio of phosphorylated/total protein for each kinase averaged for 4 donors and normalized to control (CTL) group. *, $P<0.05$ vs. CTL; $^{\#}$ $P<0.05$ vs. 1Hz.

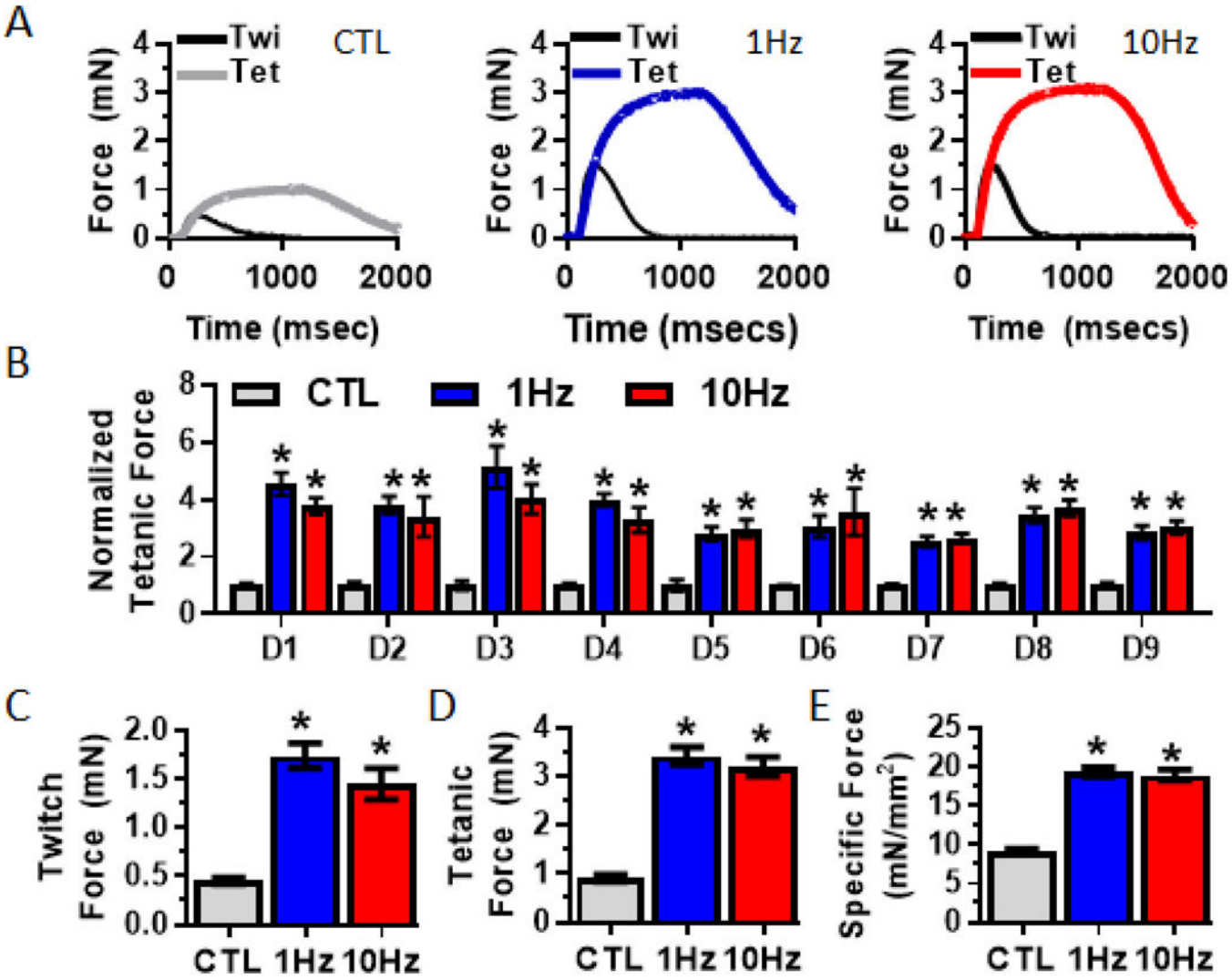

Figure 5. Effects of electrical stimulation on myobundle force generation.

(**A**) Representative twitch and peak tetanic (20Hz) force traces in 2-week myobundles that were either unstimulated (CTL) or electrically stimulated using the 1Hz or 10Hz protocols. (**B**) Normalized peak tetanic force generation from 9 independent donors (D1 – 9) (n = 4 – 22 myobundles per donor per group). (**C-D**) Average peak (**C**) twitch and (**D**) tetanic forces from all donors (n= 66 – from N = 9 myobundles per group). (**E**) Specific force generation (n=16 – 32 myobundles f rom N = 4 donors per group). *, P<0.01 vs. CTL.

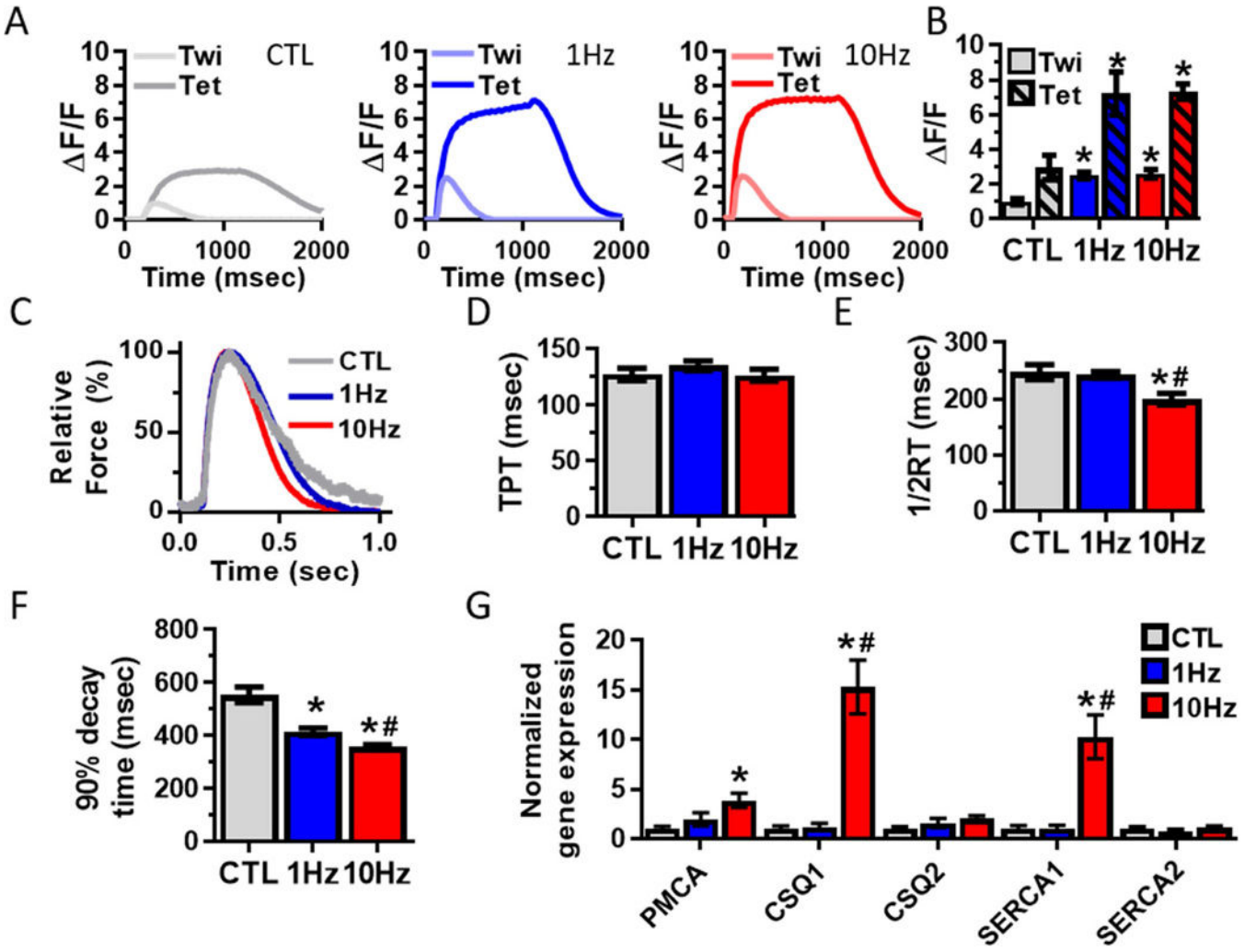

Figure 6. Effects of electrical stimulation on calcium handling in myobundles.

(**A**) Representative traces of gCaMP6-reported Ca^{2+} transient signal from myobundles stimulated at 1Hz (twitch) and 20Hz (tetanus). (**B**) Quantified amplitudes of Ca^{2+} transients (n = 12 myobundles from N = 3 donors per group). (**C**) Representative twitch traces in non-stimulated (CTL) and 1 and 10Hz stimulated myobundles. (**D**) Time-to-peak tension (TPT), (**E**) Half-relaxation time (1/2RT) and (**F**) 90% decay time (n = 66 – 98 myobundles from N = 9 donors per group). (**G**)Quantified mRNA expression of calcium-handling related genes (n = 9 – 12 myobundles from N = 3 donors per group). *, P<0.05 vs. CTL; $^{\#}$, P<0.05 vs. 1Hz.

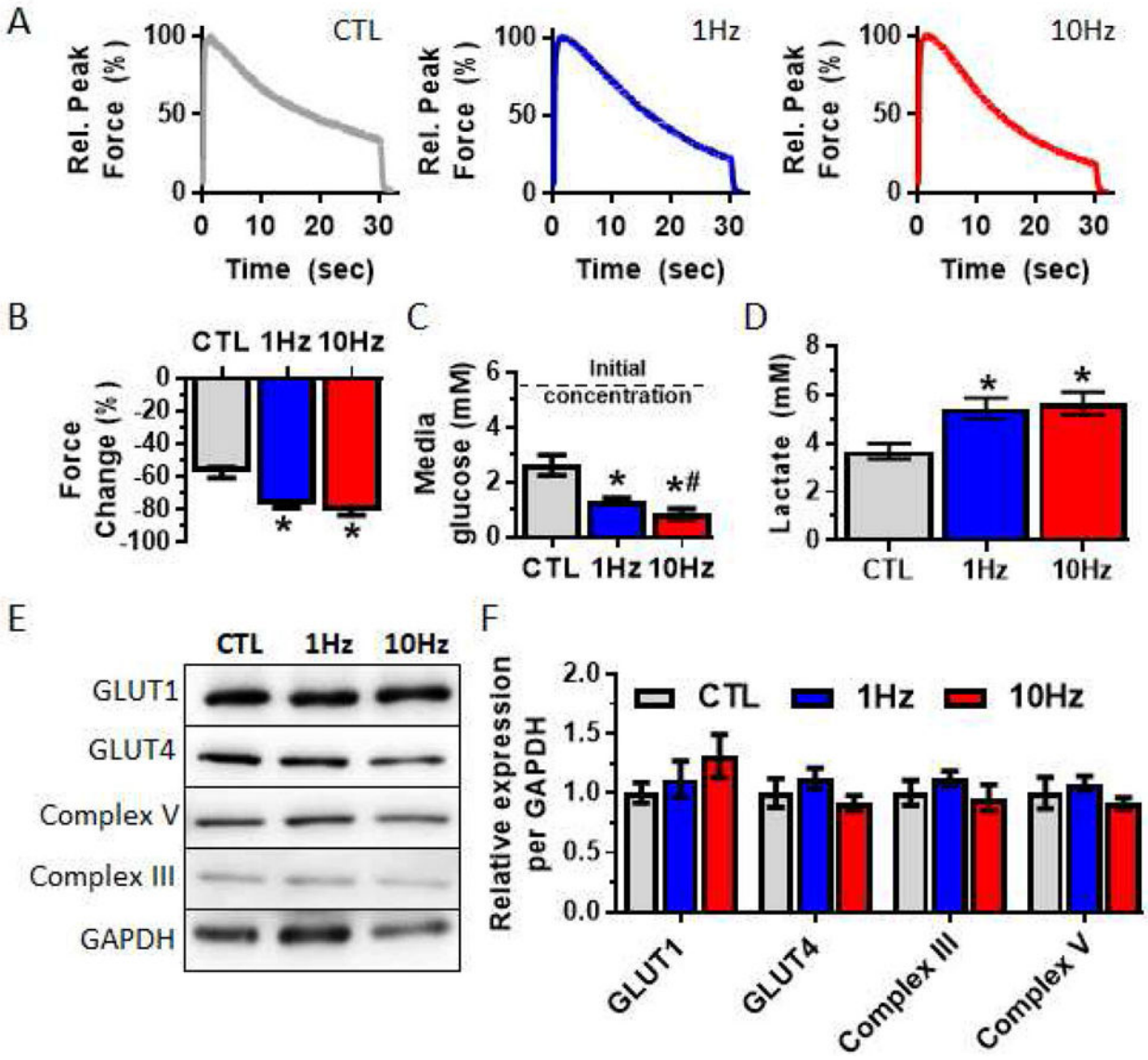

Figure 7. Effects of electrical stimulation on fatigue and metabolic function of myobundles.

(**A**) Representative traces of tetanic contraction in response to a 30-s fatiguing stimulus (20Hz). (**B**) Force loss from the onset to the end of a fatiguing contraction (n = 18 – 32 myobundles from N = 3 donors). (**C**) Media glucose concentration following 24-hr culture of 2-week old myobundles; lower glucose concentration indicates higher glucose utilization (n = 16 myobundles from N = 4 donors). (**D**) Media lactate concentration following 24-hr culture of 2-week old myobundles (n = 16 myobundles from N = 4 donors). (**E**) Representative Western blots of metabolic proteins. (**F**) Quantification of protein expression (n = 9 myobundles from 3 donors). *, $P<0.05$ vs. CTL; $^{\#}$, $P<0.05$ vs. 1Hz.

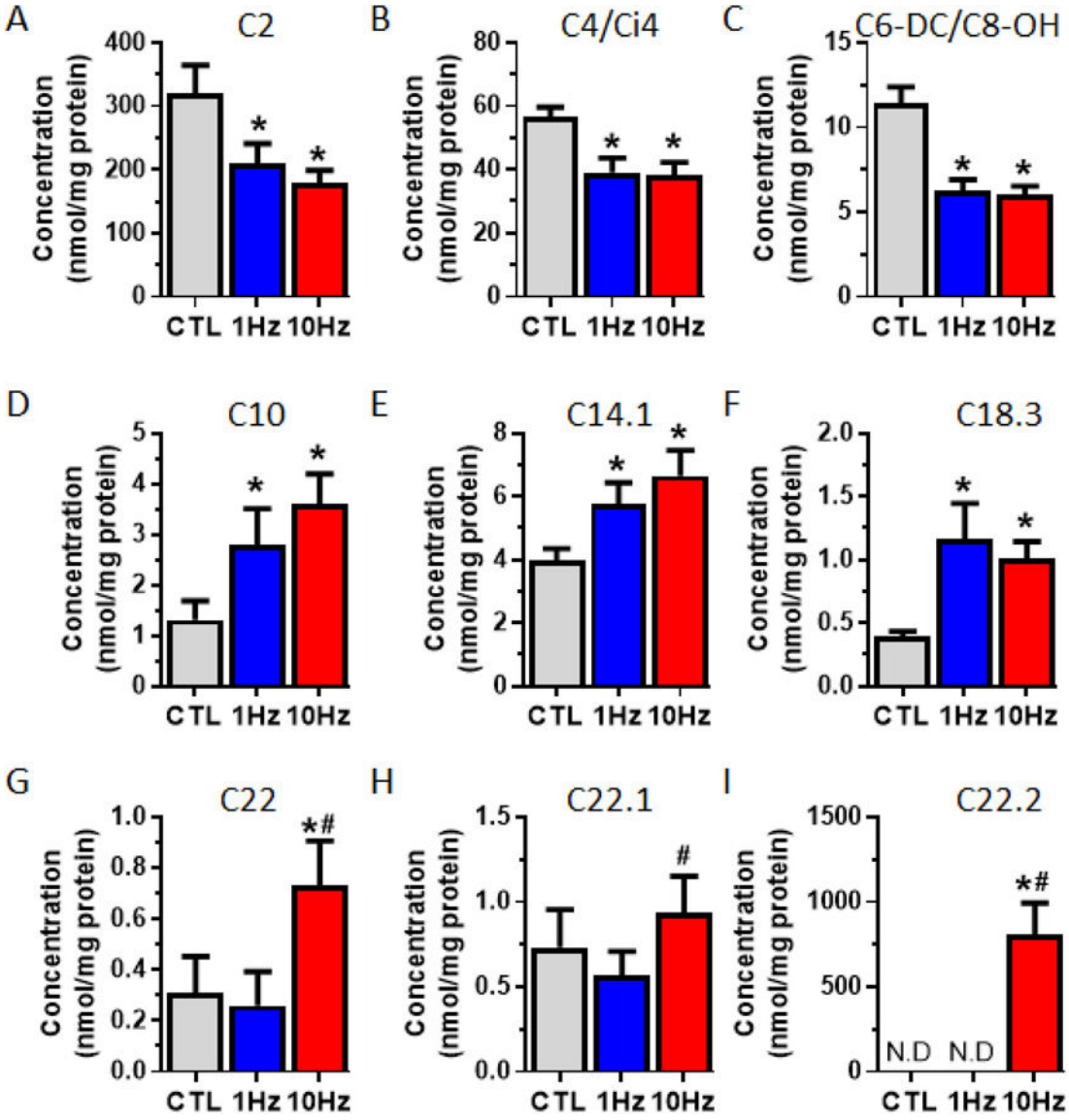

Figure 8. Effects of electrical stimulation on the concentrations of intracellular acylcarnitine species in myobundles.

2-week myobundles were collected immediately following the last bout of stimulation for. (**A-I**) Intracellular concentration of (**A**) acetylcarnitine, (**B-C**) short-chain, (**D-E**) medium-chain, and (**F-I**) long-chain acylcarnitines. (N = 1 donor, n = 6 myobundles per group). *, $P<0.05$ vs. CTL; #, $P<0.05$ vs. 1Hz.